Analysis of standing sound waves using holographic interferometry

Daniel A. Russell,[a] David E. Parker, and Russell S. Hughes[b]
Department of Physics, Kettering University, Flint, Michigan 48504

(Received 5 December 2008; accepted 12 May 2009)

Optical holographic interferometry was used to study standing sound waves in air inside a resonance tube driven by a small loudspeaker at one end. The front face of the resonance tube was constructed with plexiglass, allowing optical interrogation of the tube interior. The object beam of the holographic setup was directed through the plexiglass and reflected off the back wall of the resonator. When driven at resonance, the fluctuations in the air density at the antinodes altered the refractive index of the air in the tube, causing interference patterns in the resulting holographic images. Real-time holography was used to determine resonance frequencies and to measure the wavelengths of the standing waves. Time-average holography was used to observe the effect of increasing the sound pressure level on the resulting fringe pattern. A simple theory was developed to successfully predict the fringe pattern.
[DOI: 10.1119/1.3147683]

I. INTRODUCTION

More than 40 years ago Powell and Stetson[1,2] described time-average and real-time[3] techniques of holographic interferometry and their usefulness in analyzing the steady state vibration of small objects. Since then, time-average holographic interferograms have become useful tools for the vibrational analysis of musical instruments,[4–6] and double exposure holographic interferometry has been used to analyze transient vibrations[7] as well as liquid diffusion[8] and air flow.[9] The accessibility of holographic interferometry in the undergraduate laboratory has been demonstrated by several papers.[10–13]

Salant *et al.*[14] demonstrated that a transparent standing sound wave with sufficient amplitude in air can produce fringes on a time-average holographic image. More recently, Peterson *et al.*[15] used stroboscopic holographic interferometry to produce real-time images of the pressure field inside a resonance tube. They used an air-filled wedge-shaped cell to superpose carrier fringes on the resulting interference pattern. By strobing the laser beam they were able to effectively observe the standing wave oscillate.

In this paper we describe an experiment that uses both real-time and time-average holographic interferometries to study standing waves in a resonance tube. We used real-time holography to locate the pressure nodes and antinodes of the harmonic sequence of standing waves in the tube and to measure the wavelengths of the standing waves. Time-average holography was used to study how the fringe pattern changed when the intensity of the sound wave increased. A simple prediction of the time-average fringe patterns was developed and found to agree with experimental measurements.

II. EXPERIMENTAL SETUP

The experiment used a typical holography setup as shown in Fig. 1. The light source was a 50 mW He–Ne laser (λ=633 nm). The object and reference beams were expanded with a pinhole lens system. The object beam was further spread in the horizontal direction by a plano-concave cylindrical lens to better illuminate the resonance tube. A transmission hologram was recorded with a Newport thermoplastic holographic camera, which records and develops the holographic image on a thermoplastic plate *in situ*. A video camera was used to look through the thermoplastic plate toward the object to record holographic images and fringe patterns on video tape for later analysis.

In the experiments described in Refs. 14 and 15 the object beam was projected directly through the resonance tube before falling on the holographic plate. We used a resonance tube with only one transparent face and reflected the object beam off the back wall of the resonance tube, which had been painted with flat white paint. Reflecting the object beam off the back wall of the resonance tube had the advantageous effect of allowing the observation of fringes in a time-average hologram for sound pressure levels below 150 dB instead of 165 dB as reported in Refs. 14 and 15. This difference is significant because once the sound pressure level exceeds 150 dB, sinusoidal sound waves begin to change their shape due to nonlinear effects and the speed of sound begins to depend on the pressure amplitude. Keeping the sound pressure levels low enabled us to predict the fringe patterns without having to include nonlinear effects in the theory.

Figure 2 shows a close-up photo of the resonance tube used in this experiment. The tube interior has a length of L_x=61.0 cm, a rectangular cross-section of L_y=6.4 cm and L_z=7.0 cm. The top, bottom, and back walls were made from 0.25 in. steel, both ends were 0.5 in. steel, and the transparent front face was 0.5 in. plexiglass. A ruled grating was attached to the outside of the tube so fringe widths and wavelengths could be measured. The horn driver was connected to the resonance tube with a fitted coupling that screwed into the 0.5 in. steel plate end wall. The sound pressure levels inside the tube were measured by inserting a 0.25 in. diameter B&K type 4156 high-intensity microphone through a hole drilled into the end of the tube opposite the driver. The output of the microphone was observed in the frequency domain using a Stanford Research Systems SR785 FFT analyzer. The microphone-analyzer system was calibrated to a 124 dB signal at 250 Hz using a B&K 5152 pistonphone. The resonance frequencies of the resonance tube were determined using the swept-sine analysis feature of the frequency analyzer with a frequency resolution of $\pm$2 Hz.

The measured resonance frequencies are plotted in Fig. 3

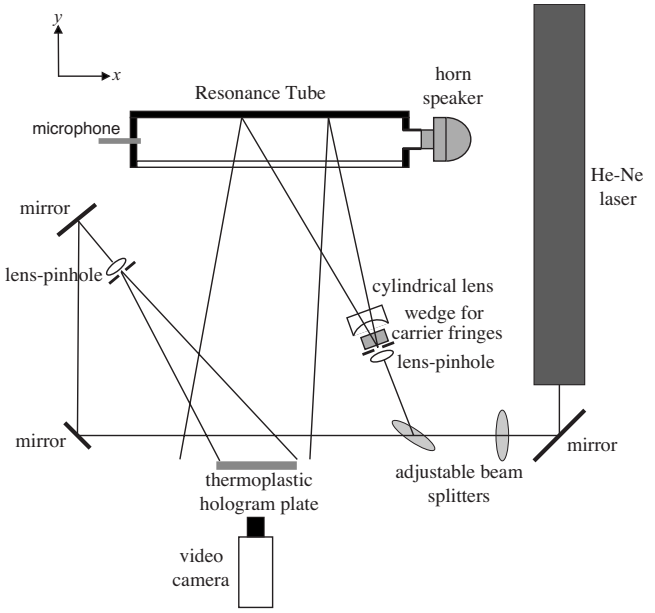

Fig. 1. Diagram of holography system used to observe standing sound waves.

as a function of mode number n. The dashed trendline in the plot represents the calculated resonance frequencies of a closed-closed tube of length $L_x=0.61$ m,

$$f_n = \frac{nc}{2L_x}, \tag{1}$$

with $c=342$ m/s, corresponding to the speed of sound in the laboratory environment at a temperature of 18 °C. The horizontal line in Fig. 3 indicates the cutoff frequency,[16,17] above which it is no longer guaranteed that only plane waves will exist. The cutoff frequency depends on the depth L_y and height L_z of the tube,

$$f_{\text{cutoff}} = \frac{c}{2\pi}\sqrt{\left(\frac{\ell\pi}{L_y}\right)^2 + \left(\frac{m\pi}{L_z}\right)^2}, \tag{2}$$

where ℓ and m are integers used to identify modes in which the cross-sectional distribution of pressure varies due to standing waves between the side walls of the waveguide. According to Eq. (2) the first nonplane wave mode ($\ell=0$, $m=1$) was expected at 2443 Hz, so we were guaranteed to observe plane waves only below this frequency. The holographic images discussed later in this paper are for the $n=6$ plane wave mode that was experimentally observed at 1698 ± 2 Hz, which is within 1% of the theoretical value.

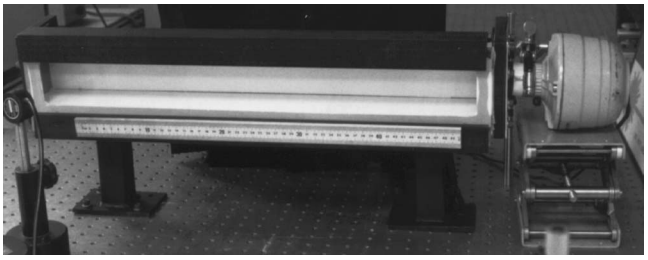

Fig. 2. Photograph of the resonance tube with dimensions of $L_x=61.0$ cm, $L_y=6.4$ cm, and $L_z=7.0$ cm.

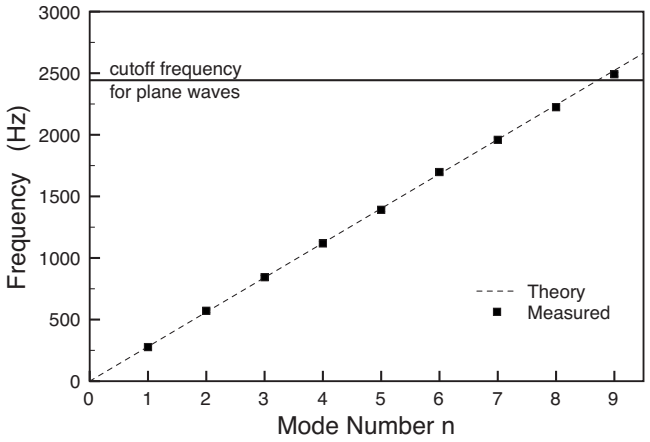

Fig. 3. Measured resonance frequencies (±2 Hz) versus mode number for the resonance tube.

III. REAL-TIME HOLOGRAPHIC INTERFEROGRAMS

Real-time holographic interferometry is useful for real-time observation of slow changes in the refractive index of a material[8] and small static deflections of an object.[18] For this experiment it provided a means of visualizing the standing sound wave inside the resonance tube. First, a phase hologram of the resonance tube was recorded onto the thermoplastic plate with the sound turned off. The holographic image was then viewed with the object beam still on so that the virtual object viewed through the hologram was superimposed on the actual object. Carrier fringes were added to the holographic image by displacing the object beam via rotation of a glass wedge inserted in front of the object beam pinhole, as shown in Fig. 1. When viewing a real-time hologram, any slight deflection of the object causes the carrier fringes to move, and a steady state vibration causes the carrier fringes to blur. In our case the carrier fringes blurred because the effective object path length varied due to changes in the refractive index as the pressure amplitude of the standing wave oscillated sinusoidally inside the resonator tube. Petersen *et al.*[15] used an acoustic-optic modulator to strobe their laser so that the object was illuminated once per cycle of the standing wave, effectively freezing the carrier fringes in place. They were able to watch the strobed carrier fringes shift position as the amplitude of the sound wave was increased. In our experiment we utilized the blurring of the carrier fringes to locate the pressure antinodes in the standing wave patterns and measure the wavelengths.

Figure 4 shows a video screen capture of the real-time holographic image obtained for the standing wave with frequency of 1698 Hz, corresponding to the $n=6$ mode of the resonance tube. Figure 4(a) shows the carrier fringes with the sound turned off. In Fig. 4(b) the sound level inside the resonance tube was 140 dB and the carrier fringes are blurred at regular intervals. The regions where the carrier fringes remain visible correspond to pressure nodes where the pressure and refractive index do not change, and the effective path length of the object beam is unaffected by the sound wave. The regions where the carrier fringes are blurred correspond to pressure antinodes where the pressure and refractive index alternate between maximum and minimum values at the resonance frequency. The distance between two blurred regions (two antinodes) equals half a wavelength.

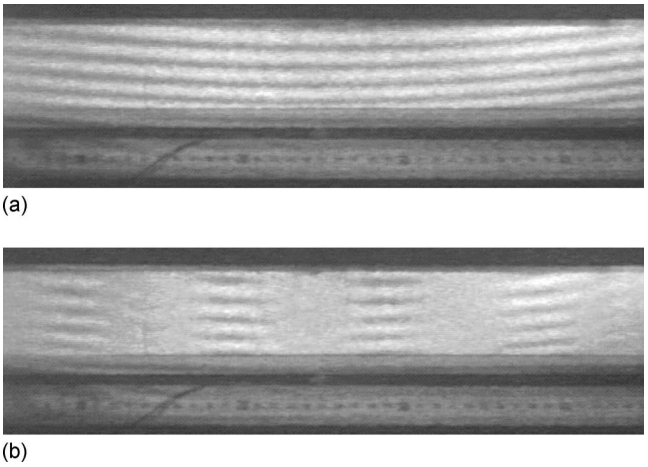

Fig. 4. Real-time holograms with carrier fringes of the resonance tube with (a) the sound turned off and (b) with a 1698 Hz ($n=6$) standing wave at 140 dB (bottom).

Figure 5 shows the wavelengths obtained by measuring the distance between antinodes of the real-time holograms as a function of mode number n. The dashed curve represents the expected wavelengths according to $\lambda=2L_x/n$. The error bars on the measured data points indicate the uncertainty in locating the exact center of the blurred regions in the real-time holograms.

IV. TIME-AVERAGE HOLOGRAPHIC INTERFEROGRAMS

Time-average holograms were made by exposing the thermoplastic plate for a long time relative to the period of the standing wave. After the plate was developed the holographic image was viewed with the object beam turned off and the fringe pattern was recorded using a video camera. A number of holograms were made for several of the resonance frequencies of the tube and with increasing sound pressure levels at each frequency. Frame grabber software was used to capture single frame images for further analysis.

Figure 6 illustrates how the time-average holographic images for the 1698 Hz, $n=6$ mode changed with increasing sound pressure level. The hologram in Fig. 6(a) corresponds to a sound pressure level of 140 dB and shows two white fringes located at nodes where the pressure and thus the refractive index do not change. The dark fringes are located at antinodes where the pressure and refractive index oscillate with maximum amplitude. As the sound level increases, the two bright regions grow narrower, but their locations do not change because they are located at pressure nodes. The hologram in Fig. 6(b) corresponds to a sound level of 145 dB. The dark fringe at the antinode has split and a bright fringe now appears at the antinode. The irradiance of this new bright fringe is much lower than the bright stationary regions at the nodes. Increasing the sound level further to 149 dB in Fig. 6(c) causes a new dark fringe to appear. This dark fringe is itself split and replaced with an additional bright fringe as the sound level increases to 151 dB in Fig. 6(d). The three-dimensional aspect of the standing wave is evident in Figs. 6(c) and 6(d), which show semicircular fringe patterns on the floor of the resonance tube. This pattern is further illustrated in Fig. 7.

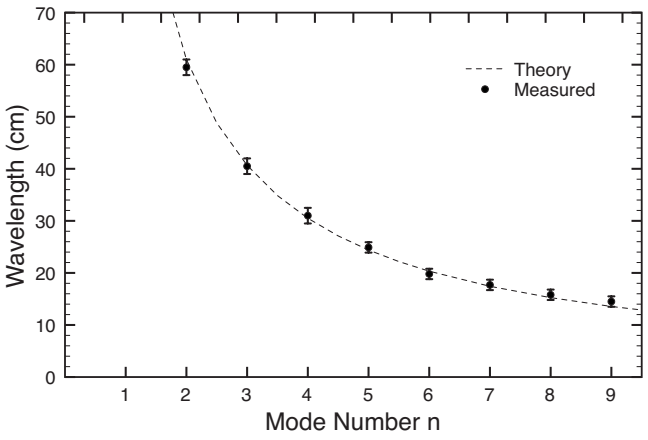

Fig. 5. Wavelength as a function of mode number as measured from the distance between blurred carrier fringes on a real-time hologram compared with theory (dashed curve) for a closed-closed tube.

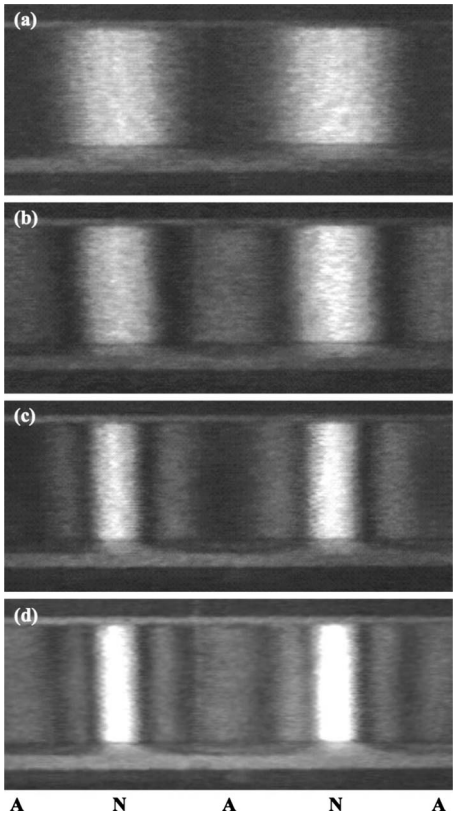

Fig. 6. Time-average holographic images for the 1698 Hz ($n=6$) standing wave mode corresponding to sound pressure levels of (a) 142, (b) 145, (c) 149, and (d) 151 dB. Nodes and antinodes are indicated by N and A, respectively.

V. THEORETICAL FRINGE PATTERNS

Other papers describing undergraduate experiments with holographic interferometry[12,13] have used a simple theory to predict the number of fringes as a function of vibrational amplitude for comparison with measured fringe counts. Because the vibrating object in this experiment is a standing wave in air, it was simple to predict the actual profiles of the fringe patterns, not just the number of fringes. A potential

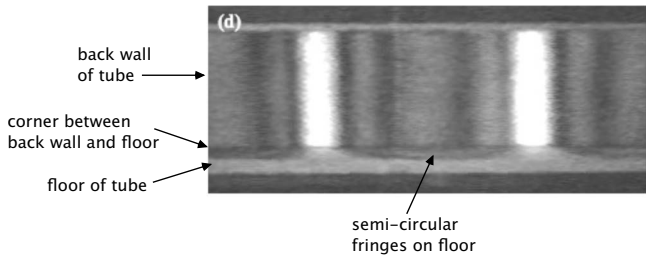

Fig. 7. The three-dimensional nature of the time-average holograms in Fig. 6 is evidenced by the semicircular fringes on the floor of the resonance tube.

limitation to such a prediction is the fact that the sound pressure levels in question are in the range where nonlinear effects might not be ignorable.

The total pressure associated with a finite amplitude standing sound wave in a resonance tube of length L_x and closed at both ends may be expressed as[19]

$$p(x,t) = P_0 + 2p_m \cos\left(\frac{m\pi}{L_x}x\right)\sin(\omega t), \tag{3}$$

where P_0 is atmospheric pressure, $2p_m$ is the peak pressure amplitude fluctuation due to the standing sound wave, and x is the distance from one of the rigid ends of the tube. The alternating regions of higher and lower pressure cause the refractive index of the gas to change accordingly. A time-average hologram measures irradiance, which depends on the square of the amplitude of the light falling on the hologram plate. Because the time average of $\sin^2(\omega t)$ equals 1/2, the time dependence in Eq. (3) does not matter, and we need only be concerned with the dependence on position x to predict the fringe pattern.

The refractive index n for air may be calculated from the relation[20]

$$(n-1)\times 10^8 = 8342.13 + \frac{2\,406\,030}{130-\sigma^2} + \frac{15\,997}{38.9-\sigma^2}, \tag{4}$$

where $\sigma = 1/\lambda_{\text{vac}}$ and λ_{vac} has units of μm. If the air is at temperature T in °C and pressure P in pascal, the value in Eq. (4) should be multiplied by[20]

$$\frac{P[1+P(61.3-T)\times 10^{-10}]}{96\,095.4(1+0.003\,661T)}. \tag{5}$$

As an example, for light from a He–Ne laser ($\lambda_{\text{vac}}=0.633$ μm) in dry standard air at 18 °C and (atmospheric) pressure of 101.325 kPa, the index of refraction is $n=1.000\,273\,66$.

Because of the standing sound wave in Eq. (3), the pressure term in Eq. (5) varies with location x along the length of the resonance tube. This variation means that the index of refraction in Eq. (4) is a function of position $n(x)$. It is this positional variation in the index of refraction that is responsible for the blurring of carrier fringes on a real-time holographic image as well as the fringe patterns on a time-average holographic image. The fringes observed in a reconstructed time-average holographic image are due to the time-average of the phase shift ϕ in the object beam due to the refractive index variation in the resonance tube when the hologram is generated. A phase shift of 2π corresponds to a change in object beam path length of one wavelength λ. So the phase shift of the object beam is predicted by

$$\frac{\phi}{2\pi} = \frac{2L_y\Delta n}{\lambda}, \tag{6}$$

where Δn represents the change in the refractive index of air due to the standing wave and L_y is the resonance tube depth. The factor $2L_y$ indicates that the object beam passes through the sound field twice, reflecting off the back wall of the resonance tube. It has been assumed that the object beam light incident on the resonance tube and object beam light reflected back toward the hologram are approximately perpendicular to the front face of the tube. To account for the spatial dependence of the refractive index, we write the phase difference as

$$\phi(x) = 4\pi\frac{L_y\Delta n(x)}{\lambda}. \tag{7}$$

During the recording of a time-average hologram the phase information is recorded as the average of $\phi(x)$. If $I_0(x)$ is the reconstructed holographic image irradiance produced by a hologram with no standing wave present in the resonance tube, then the holographic image irradiance with a standing wave present is[18]

$$I(x) = I_0(x)J_0^2(|\phi(x)|), \tag{8}$$

where $|\phi(x)|$ indicates taking the magnitude of the phase shift due to the refractive index difference and J_0 is the zero order Bessel function.

The peak pressure amplitude in the tube was calculated from the measured sound pressure level L_p in decibels,

$$p_m = \sqrt{2}p_{\text{ref}}10^{L_p/20}, \tag{9}$$

where $p_{\text{ref}}=20\times 10^{-6}$ Pa and the $\sqrt{2}$ indicates the conversion from rms to peak amplitude. Theoretical predictions of the fringe pattern irradiance for time-average holograms were calculated using Eqs. (3)–(5) and (7)–(9).

Figure 8 shows the predicted fringe patterns as functions of position for the same sound pressure levels as the measured fringe patterns shown in Fig. 6. The horizontal axis in Fig. 8 covers the same distance shown in the photographs in Fig. 6. The dashed curve in each plot in Fig. 8 represents the magnitude of the pressure standing wave (zero at nodes and maximum at antinodes). The solid curves represent the fringe pattern irradiance, or the brightness of the hologram image, as predicted by Eq. (8). For a sound pressure level of 142 dB, Fig. 8(a) predicts bright fringes at pressure nodes with a dark fringe between at the pressure antinode. When the sound level increases to 145 dB in Fig. 8(b), a faint bright fringe appears at the pressure antinode. In Fig. 8(c), as the sound level increases to 149 dB, the faint bright fringe at the antinode has split into two faint bright fringes with a dark fringe between at the antinode. Finally, at 151 dB the bright fringes at the pressure nodes have become thinner, and another faint bright fringe appears at the pressure antinode. The agreement between the predicted fringe patterns in Fig. 8 and measured fringe patterns in Fig. 6 with respect to fringe location, width, and brightness is very good.

VI. CONCLUSION

We have described an experiment that uses real-time and time-average holographic interferograms as a tool for studying standing sound waves. Real-time holography was used to observe the standing waves and to obtain measurements of

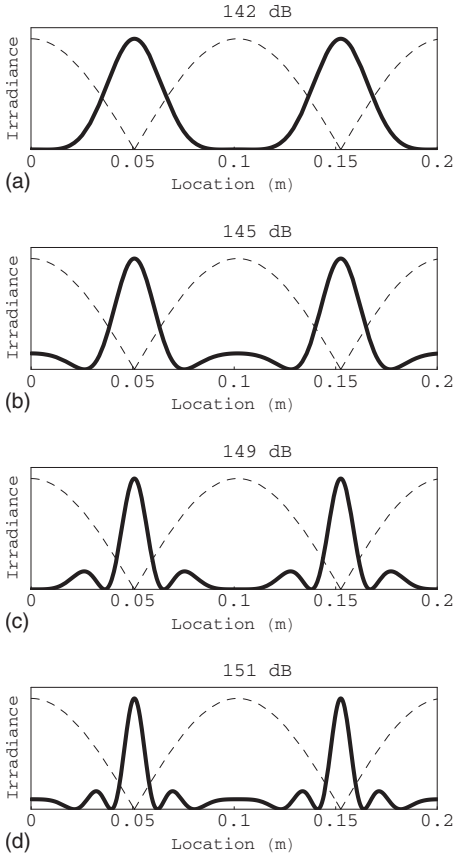

Fig. 8. Theoretical predictions of the fringe pattern irradiance corresponding to the measured fringe patterns shown in Fig. 6. The dashed curve indicates the pressure amplitude of the standing sound wave. The solid curve represents the brightness of the hologram image. The locations represent the distance from a pressure antinode.

resonance frequencies and wavelengths. Time-average holograms showed the effect of increasing the pressure amplitude on the index of refraction as evidenced by the changes in the fringe patterns. A simple prediction of the fringe pattern matched the measured patterns. The success of this simple theory is largely due to the fact that our experimental setup resulted in the appearance of fringes at sound pressure levels, which are just barely low enough that nonlinear effects may be ignored. A possible extension of this work would be to develop the theory more fully for finite amplitude sound waves including second order nonlinear effects.

ACKNOWLEDGMENTS

The authors would like to thank Newport Corporation and the General Motors Corporation for donating some of the optical equipment used in this experiment. We would also like to thank the reviewer for providing helpful comments.

[a]Electronic mail: drussell@kettering.edu
[b]This experiment began while Hughes was a senior undergraduate student. He is currently employed by Mantech (www.mantech.com).

[1] R. L. Powell and K. A. Stetson, "Interferometric vibration analysis of three-dimensional objects by wavefront reconstruction," J. Opt. Soc. Am. **55**, 612 (1965).
[2] R. L. Powell and K. A. Stetson, "Interferometric vibration analysis by wavefront reconstruction," J. Opt. Soc. Am. **55**, 1593–1598 (1965).
[3] K. A. Stetson and R. L. Powell, "Interferometric hologram evaluation and real-time vibration analysis of diffuse objects," J. Opt. Soc. Am. **55**, 1694–1695 (1965).
[4] W. Reinicke and L. Cremer, "Application of holographic interferometry to vibrations of the bodies of string instruments," J. Acoust. Soc. Am. **48**(4), 988–992 (1970).
[5] T. D. Rossing and D. S. Hamilton, "Modal analysis of musical instruments with holographic interferometry," *Applications of Optical Engineering: Proceedings of OE/Midwest '90*, [SPIE **1396**, 108–121 (1990)] (SPIE, Bellingham, WA, 1990).
[6] T. D. Rossing and H. J. Sathoff, "Modes of vibration and sound radiation from tuned handbells," J. Acoust. Soc. Am. **68**(6), 1600–1607 (1980).
[7] L. O. Heflinger, R. F. Wuerker, and R. Brooks, "Holographic interferometry," J. Appl. Phys. **37**, 642–649 (1966).
[8] H. Fenichel, H. Frankena, and F. Groen, "Experiments on diffusion in liquids using holographic interferometry," Am. J. Phys. **52**, 735–738 (1984).
[9] K.-E. Peiponen, R. Hämäläinen, and T. Asakura, "Laboratory studies of air flow visualization using holographic interferometry," Am. J. Phys. **59**(6), 541–544 (1991).
[10] K. Lubell and R. Prigo, "Production of real-time holographic interferograms," Am. J. Phys. **55**(9), 823–825 (1987).
[11] A. B. Western and R. Bahaguna, "Simplified production of real-time holographic interferograms," Am. J. Phys. **57**(6), 560–561 (1989).
[12] R. D. Bahuguna, A. B. Western, and S. Lee, "Experiment in time-average holographic interferometry for the undergraduate laboratory," Am. J. Phys. **56**(8), 718–721 (1988).
[13] K. Menou, B. Aduit, X. Boutillon, and H. Vach, "Holographic study of a vibrating bell: An undergraduate laboratory experiment," Am. J. Phys. **66**(5), 380–385 (1998).
[14] R. F. Salant, W. G. Alwang, L. A. Cavanaugh, and E. Sammartino, "Visualization of standing acoustic waves using time-average optical holographic interferometry," J. Acoust. Soc. Am. **44**(6), 1732–1733 (1968).
[15] R. W. Peterson, S. J. Pankratz, T. A. Perkins, A. Dickson, and C. Hoyt, "Holographic real-time imaging of standing waves in gases," Am. J. Phys. **64**(9), 1139–1142 (1996).
[16] D. D. Reynolds, *Engineering Principles of Acoustics, Noise and Vibration Control* (Allyn & Bacon, Boston, MA, 1981), pp. 354–359.
[17] K. Meykens, B. V. Rompaey, and H. Janssen, "Dispersion in acoustic waveguides—A teaching laboratory experiment," Am. J. Phys. **67**, 400–406 (1999).
[18] J. T. Luxon and D. E. Parker, *Industrial Lasers and Their Applications*, 2nd ed. (Prentice-Hall, Englewood Cliffs, NJ, 1992), pp. 224–230.
[19] D. E. Hall, *Basic Acoustics* (Krieger, Malabar, FL, 1993), pp. 135, 143.
[20] *CRC Handbook of Chemistry and Physics*, 95th ed. (McGraw-Hill, New York, 1994), p. 266.